Published in final edited form as:
*J Neurosci Methods*. 2014 August 15; 233: 155–165. doi:10.1016/j.jneumeth.2014.06.022.

# An electrocorticographic electrode array for simultaneous recording from medial, lateral, and intrasulcal surface of the cortex in macaque monkeys

**Makoto Fukushima**[1], **Richard C. Saunders**[1], **Matthew Mullarkey**[1], **Alexandra M. Doyle**[1], **Mortimer Mishkin**[1], and **Naotaka Fujii**[2]

[1]Laboratory of Neuropsychology, National Institute of Mental Health, National Institutes of Health, 49 Convent Drive, Bethesda, Maryland 20892, U.S.A

[2]Laboratory for Adaptive Intelligence Brain Science Institute, RIKEN, 2-1 Hirosawa, Wako, Saitama 351-0198, Japan

## Abstract

**Background—**Electrocorticography (ECoG) permits recording electrical field potentials with high spatiotemporal resolution over a large part of the cerebral cortex. Application of chronically implanted ECoG arrays in animal models provides an opportunity to investigate global spatiotemporal neural patterns and functional connectivity systematically under various experimental conditions. Although ECoG is conventionally used to cover the gyral cortical surface, recent studies have shown the feasibility of intrasulcal ECoG recordings in macaque monkeys.

**New Method—**Here we developed a new ECoG array to record neural activity simultaneously from much of the medial and lateral cortical surface of a single hemisphere, together with the supratemporal plane (STP) of the lateral sulcus in macaque monkeys. The ECoG array consisted of 256 electrodes for bipolar recording at 128 sites.

**Results—**We successfully implanted the ECoG array in the left hemisphere of three rhesus monkeys. The electrodes in the auditory and visual cortex detected robust event related potentials to auditory and visual stimuli, respectively. Bipolar recording from adjacent electrode pairs effectively eliminated chewing artifacts evident in monopolar recording, demonstrating the advantage of using the ECoG array under conditions that generate significant movement artifacts.

**Comparison with Existing Methods—**Compared with bipolar ECoG arrays previously developed for macaque monkeys, this array significantly expands the number of cortical target areas in gyral and intralsulcal cortex.

Corresponding author: Makoto Fukushima, Laboratory of Neuropsychology, National Institute of Mental Health, National Institutes of Health, Building 49, Room 1B80, 49 Convent Drive, Bethesda, MD 20892, U.S.A., makoto_fukushima@me.com, Phone: +1-301-443-7458, Fax: +1-301-402-0046.

**Conclusions—**This new ECoG array provides an opportunity to investigate global network interactions among gyral and intrasulcal cortical areas.

### Keywords

Electrocorticography; ECoG; Electrophysiology; Evoked potentials; Multielectrode; Monkey

## Introduction

The primate brain consists of multiple distinct cortical circuits underlying sensory, cognitive, and motor functions. For example, the ventral and dorsal visual cortical streams process stimulus quality and spatial location, respectively (Ungerleider and Mishkin 1982). In audition, stimulus quality and location are also processed separately along a ventral and dorsal stream respectively (Romanski et al. 1999). In each pair of auditory and visual streams, response latency increases from the primary to the higher-order sensory areas (Raiguel et al. 1989; Schmolesky et al. 1998; Bendor and Wang 2008; Kikuchi et al. 2010; Scott et al. 2011). Although this suggests that the sensory information is processed serially, the cortical subdivisions in these pathways are also connected reciprocally (Hackett 2011; Kravitz et al. 2011; 2013). The exact functions served by interactions among cortical areas have not yet been fully investigated because of the considerable technical challenges in measuring and analyzing neuronal activity with high spatiotemporal resolution from multiple brain areas. Conventionally, each cortical area has been investigated individually through electrophysiological recording of spikes and local field potentials (LFPs) by penetrating cortical tissue with single or multiple microelectrodes. Although this method can capture detailed neural responses with millisecond resolution, and it has also been used for recording from multiple cortical areas simultaneously (Truccolo et al. 2011; Feingold et al. 2012; Salazar et al. 2012), it is not ideal for recording at high spatial resolution across large extents of the cortical surface. Another approach is functional MRI, but while it can probe whole brain activity noninvasively, it does so with relatively low spatial and temporal resolution.

An alternative method that combines both high spatial and high temporal resolution is Electrocoticography (ECoG), which can record neural activity simultaneously from numerous electrodes placed on the surface of the cortex without penetrating the cortical tissue with electrodes. ECoG has been used to detect epileptogenic foci by recording LFPs across a large expanse of cortex in human patients (Palmini 2006). Also, because ECoG allows extensive coverage of the cortex, it recently has become an important experimental tool for investigating functional interactions among cortical areas underlying various sensory, motor, and cognitive functions (Canolty and Knight 2010; Beauchamp et al. 2012; Mesgarani and Chang 2012; Chang et al. 2013). There has also been increasing interest in applying ECoG to record information carried in different temporal scales e.g. gamma and theta band oscillations (Fries 2005; Edwards et al. 2009; Schroeder and Lakatos 2009; Viventi et al. 2011; Giraud and Poeppel 2012; Einevoll et al. 2013). These applications of ECoG have been made possible by recent advances in high-channel-count data acquisition and mathematical tools for analyzing high-dimensional data (Brovelli et al. 2004; Bressler and Seth 2011; Friston et al. 2012). Further, application of chronically implanted ECoG

arrays in animal models provides an opportunity to investigate global spatiotemporal neural patterns and interactions systematically under various experimental conditions (Rubehn et al. 2009; Chao et al. 2010; Bosman et al. 2012).

ECoG is applicable for recording LFPs not only from the cortical surface of a gyrus but also from the cortex buried within sulci (Yanagisawa et al. 2009; Matsuo et al. 2011; Fukushima et al. 2012). For example, major proportions of the auditory cortex in humans and macaques are imbedded in the lateral sulcus (Formisano et al. 2003; Hackett 2011). We recently developed a technique for inserting ECoG arrays into the lateral sulcus to allow recording simultaneously from primary and higher-order auditory subdivisions located on the supratemporal plane (STP) (Fukushima et al. 2012; 2014). In the current study, we combined this technique with another technique developed for an ECoG array that was designed to cover the lateral and medial gyral surfaces of the macaque cortex (Nagasaka et al. 2011).

## Material and methods

### Electrode manufacturing process

The ECoG array was manufactured and assembled by Cir-tech Inc. (Shizuoka, Japan) with microelectromechanical system (MEMS) technologies (Fig. 1). The base of the array, made of a thin, flexible, circuit board material (FELIOS, RF786W 54ET-M, Panasonic Corp., Osaka, Japan), consisted of a layer of polyimide film sandwiched between two copper layers (Fig. 1b). First, holes (0.1 mm diameter) were made with laser drilling (Model 5330, Electro scientific industries, OR, USA) at the desired locations for electrode contacts in the base material. Then the holes were copper-plated to establish electrical continuity between the copper layers. With dry etching, the copper layer on one side was shaped for electrode contacts, and the copper layer on the other side was shaped for wiring the electrode to the connector. The copper layer for wiring was insulated by covering it with a polyimide film attached with glue (CISF0515 2NKF, Nikkan industries Co. Ltd., Tokyo, Japan). Finally, all the electrode contacts were gold-plated.

### Electrode layout and design

Each recording site was a circular disk with a diameter of 0.8 mm, and the distance between two sites in a bipolar pair was 1.8 mm (Fig. 2a). The full complement of the ECoG array consisted of four compartments, each of which was attached to a separate connector (Fig. 2b). This provided flexibility in implanting one of the compartments in the lateral sulcus (see implantation procedure). Each of the four array compartments has 56–70 recording sites soldered to a narrow-pitch connector (Figs. 3a and 3b, F4S, AXT5E6026 for 60 channels or AXT5E7026 for 70 channels, Panasonic Corp., Osaka, Japan). The connector enclosure is made of peek resin (Figs. 3b and 3c).

The ‘finger’ electrode strips extended dorsoventrally or caudorostrally (e.g. compartments #1 and #3, respectively, in Fig. 2b), similar to those in an ECoG array developed previously (Rubehn et al. 2009). Although this finger design was an appropriate fit for most of the electrodes on the frontal and parietal lobes, we found it difficult to place the electrodes on

the posterior part of the occipital lobe without each electrode overlapping another, mainly due to the extreme curvature at the occipital pole in both dorsoventral and caudorostral directions. Because this pole could be approximately modeled as part of a sphere, we designed a fan-shaped electrode array (compartment #2, Fig. 2b), which fit tightly to the spherical curvature of the pole (Fig. 6a).

## Impedance measurement

Impedances of all 256 sites in the ECoG array were measured at Unique Medical Co. Ltd. (Tokyo, Japan). The array, together with a gold reference electrode, was placed in 0.9% saline solution at room temperature. The electrode was serially connected to a resistor with known resistance values (1kΩ for 10 and 100 Hz and 1 MΩ for 1 and 10 kHz, $R_0$ in Fig. 4a), to form a simple voltage divider circuit (Fig. 4a). Sinusoidally-modulated voltage with 0.1 mV RMS ($V_{in}$ in Fig. 4a) was applied through a signal generator (AG-203 CR oscillator, Kenwood, Tokyo, Japan). Then the output voltage ($V_{out}$ in Fig. 4a) was measured with an analog voltage meter (Kikusui Electronics Corp., Kanagawa, Japan) coupled with a high input impedance amplifier (>1 GΩ, Unique Medical Co. Ltd., Tokyo, Japan) to calculate the impedance value of each of the 256 electrodes.

## Subjects

We used three adult male rhesus monkeys (*Macaca mulatta*), weighing 5–10 kg. All procedures and animal care were conducted in accordance with the Institute of Laboratory Animal Resources Guide for the Care and Use of Laboratory Animals, and all experimental procedures were approved by the National Institute of Mental Health Animal Care and Use Committee.

## Implantation procedure

The monkey was pretreated with dexamethasone (0.5–1 mg/kg at 3 mg/ml) and an antibiotic (Ditrim, 24% solution, 0.1 ml/kg i.m.) 24 hours prior to surgery and fasted for 12 hours before surgery. On the day of surgery, the animal was initially sedated with ketamine (10 mg/kg i.m.) and surgical anesthesia achieved with isoflurane (1–4% to effect). Throughout surgery, vital signs were monitored, including SpO2 and heart and respiration rates, and the animal was kept warm with a heating pad and hydrated (Ringer's solution i.v.). Mannitol (30%, 30 cc i.v. over 20 min) was infused to counteract edema and reduce brain volume. Standard sterile neurosurgical procedures were used throughout the operation.

The zygomatic arch was removed and the temporalis muscle was retracted ventrally to allow exposure of a large section of the lateral cortex of one hemisphere after a large bone flap was removed. The cranial opening extended 4–5 mm past the midline laterally to the temporal fossa below the zygomatic arch and rostrocaudally from the brow to the occipital ridge (Fig. 5). The dura was opened and reflected dorsally to expose the lateral cortical surface, and the banks of the lateral sulcus were carefully separated along its caudorostral length with a fine forceps and a small glass pipette attached to a vacuum pump. This sulcal separation extended as far medially as the circular sulcus, with special care taken to avoid penetrating the pial surface of the STP. or compromising blood vessels bridging the lips and banks of the sulcus. Bleeding was seldom a problem, but minor bleeds were controlled by

covering the vessels with small saline-soaked cottonoid patties. Compartment #1 (Fig. 2b) was separated from the other compartments and inserted in the lateral sulcus. Moistened in saline, the compartment slid easily along the sulcal surface. In some cases the placement of the array on the sulcal surface was limited by the location of sulcus-bridging vessels. The most caudal of the three arrays in compartment #1 was inserted first and aimed at area A1 by positioning its rostral edge just caudal to an (imaginary) extension of the central sulcus. This imaginary extension was in close proximity to a small bump on the STP, both being markers of A1's approximate location. The second and third arrays were then inserted immediately rostral to the first array and adjacent to each other while minimizing inter-array gaps. We then temporarily secured the rest of compartment #1 outside of the lateral sulcus on the reflected temporalis muscle (Fig. 5a).

Compartments #2–4 were placed on the lateral surface while ensuring that the three cables of compartment #1 emerging from the lateral sulcus exited from the spaces between the 'fingers' of the arrays on the lateral surface (as indicated by the yellow arrows in Figs. 5a and 5b). After compartments #2–4 were placed on the lateral surface, compartment #1 was released from the temporalis muscle so that the rest of its electrodes could be placed on the medial wall and dorsolateral surface of the prefrontal cortex. With the dura reflected, the left and right hemispheres were carefully separated with a small (4–5 mm) flat, stainless steel brain spoon to allow insertion of a part of compartment #1 onto the medial wall of the prefrontal cortex (see Fig. 2a). Small veins between the hemispheres were cauterized, but large veins were left intact. The array was then slid into position working around these remaining veins. The connector for compartment #1 was fixed to the connector enclosure (Fig. 3), the connectors for compartments #2–4 having been glued to the enclosure prior to surgery. Each cable had sufficient length to allow for individual anatomical differences. During the implantation, the cables were temporarily bundled with suture thread and placed near the bottom of the connector enclosure (Fig. 5b), so that the cables were organized as they extended out from the dural and bone flaps after the implantation. This also helped fit the cables to the curvature of the cortex during the implantation (Fig. 5b). The dural opening was then carefully sutured, the bone flap was reattached, and the cables outside of the flap were secured to the base of the connector enclosure with bone cement. Reference and ground electrodes were on compartment #3 and placed in the subdural and epidural spaces, respectively (Figs. 5b and 5c). The connector enclosure was glued (Triad Gel, Dentsply Prosthetics Inc., PA, USA) to the skull immediately adjacent to the cranial opening (Fig. 5c). Ceramic screws and bone cement were used to fix the connector enclosure to the skull, and the skin was closed in anatomical layers. Postsurgical analgesics were provided as needed in consultation with the facility veterinarian. Dexamethasone (0.5–1 mg/kg at 3mg/ml) was administered for 6 days postoperatively (three times per day for the first three days, twice per day for the following two days, and once on the last day).

## Electrophysiological recording and stimulus presentation

During an experimental session, the monkey was seated in a primate chair inside a sound-attenuating booth (Biocoustics Instruments, Inc. MD, USA). We monitored the monkey's behavioral state through a video camera and microphone connected to a PC. Auditory or visual stimuli were presented while the monkey sat calmly with its head fixed. The sound

stimuli were loaded digitally into a RZ2 base station (50 kHz sampling rate, 24 bit D/A; Tucker Davis Technology Inc., FL, USA) and presented through a calibrated free-field speaker (Reveal 501A, Tannoy, Scotland, UK) located 50 cm in front of the animal. The visual stimulus presentation was controlled by Open Ex software (Tucker Davis Technology Inc., FL, USA) and a toolbox package (Monkeylogic, http://www.brown.edu/Research/monkeylogic/ (Asaad and Eskandar 2008) for MATLAB® (The Mathworks Inc., MA, USA). The visual stimulus was a white square that filled the entire screen of a small LCD monitor (Lilliput 7″, Viviteq Inc. CA, USA) located 40 cm in front of the animal. This visual stimulus was presented 100 times for 1 second each with an inter-stimulus interval of 10 seconds (fixation was not required). The auditory stimulus was a harmonic complex tone with a fundamental frequency of 500 Hz. It was presented 100 times for 74 msec each, with an interstimulus interval of 3 seconds. The field potentials from the 256 channels of the ECoG array were recorded as a single-ended (monopolar) configuration, band-passed between 2 and 500 Hz, and digitally sampled at 1500 Hz.

## Data analysis

MATLAB® (The Mathworks Inc., MA, USA) was used for offline analysis of the field-potential data. The signal was low-pass filtered and down-sampled to 500 Hz to speed up the calculations and to reduce the computer memory requirement for the analysis. Locally re-referenced signal was obtained by subtracting one electrode from another of each bipolar pair.

## Confirmation of electrodes location

We estimated the locations of the implanted electrodes from a postoperative CT scan of the head, co-registered to a preoperative T1-weighted anatomical MR image using AFNI (Cox 1996) (Fig. 6). We used a function in AFNI that implements a method for co-registering functional and structural MRI images (Saad et al. 2009). This alignment depends primarily on matching the location of the skull bones, which are visible in both MR and CT images. Some parts of the skull, however, had been removed or displaced during the surgery for electrode implantation, and thus the alignment had to be adjusted manually using ‘Nudge’ option in AFNI to ensure that the locations of the bone in both images were aligned properly. After the alignment, the electrodes in the lateral sulcus and medial wall were visualized by orienting the image to obtain a section that included target electrodes (Fig. 6b and 6c). To view the electrodes on the lateral surface, the skull in CT and MRI images was stripped, and the co-registered CT-MR image was volume-rendered with AFNI (Fig. 6a).

## Evaluation for chewing artifacts

To evaluate chewing artifacts during mastication, we recorded ECoG signals while the monkey was chewing either a raisin or banana chip. We evaluated chewing artifacts in the visual cortex where no motor or auditory neural response was expected during mastication. To detect the artifacts, we used the squared difference between the raw and smoothed ECoG signals ($\Delta^2$) (Shimoda et al. 2012) (Fig. 8). For this calculation, the signals were smoothed by convolving them with a Chebyshev window (10 ms window length, 10 dB stop-band).

## Results

The new ECoG array enabled recording from numerous cortical areas covering most of the lateral surface and the STP in the lateral sulcus simultaneously. The new ECoG array consists of 256 recording sites for bipolar recording at 128 locations: the electrodes on the medial wall (26 sites) were arranged to cover the medial frontal, cingulate, and supplementary motor areas; the electrodes on the lateral surface (212 sites) were arranged to cover the frontal, temporal, parietal, and occipital lobes; and the electrodes in the lateral sulcus (18 sites) were designed to cover more than 2 cm along the caudorostral extent of the STP. We successfully implanted this new ECoG array in the left hemisphere of three rhesus monkeys. In one of them, recording properties of the array were evaluated by measuring the impedance of the electrodes, recording auditory and visual evoked potentials, and comparing chewing artifacts recorded with monopolar and bipolar electrode configurations.

### Electrode assembly and impedance measurement in vitro

The four compartments of the ECoG array were assembled with a connector enclosure that stored the four connectors (Fig. 3a). The size of the connector enclosure (23 mm W x 21 mm H x 6 mm D) is relatively small, for the 256 channels they contain (Fig. 3b). Two narrow-pitch connectors were stored in each of two sides of the enclosure (Fig. 3c). The footprint of the enclosure is 230 $mm^2$ (10 mm x 23 mm). This construction saves space on the skull for additional implants as necessary. To fit into this small enclosure, the cables from each array were bundled together. The total cable width at the bottom of the enclosure was 15 mm (Fig. 3c).

We measured the impedance of each of the 256 electrodes in the array *in vitro* to obtain functional characteristics of the array (see Material and methods). The impedance value for all the electrodes decreased from 10 Hz to 10 kHz, approximately following the power-law function (Fig. 4b, blue line). The mean impedance values ranged from 140 kΩ (at 10 Hz) to 0.9 kΩ (at 10 kHz), which are comparable to those in an ECoG array developed earlier for monkeys (Rubehn et al. 2009). These impedance values are much lower than the input impedance of the headstage we used for in-vivo recording (100 TΩ, LP16CH, Tucker Davis Technology Inc., FL, USA), which was needed to obtain high amplitude signal with low phase shift (Nelson et al. 2008; Rubehn et al. 2009).

### Estimation of implanted locations in vivo with CT and MR scans

After the ECoG array was successfully implanted (Fig. 5, see Material and methods), a head CT scan was obtained and co-registered with MR images to identify the location of the electrodes (Fig. 6, see Material and methods). The electrodes on the lateral surface covered many cortical areas including: dorsal and ventral prefrontal cortex, dorsal and ventral premotor cortex, primary motor cortex, caudal and rostral superior temporal gyrus, and visual cortex of the occipital lobe (Fig. 6a). The electrodes in the lateral sulcus were placed on the primary and higher-order auditory areas in caudal and rostral portions, respectively, of the supratemporal plane (Fig. 6b). On the medial wall, the electrodes covered the supplementary motor area (SMA), pre-SMA, and medial prefrontal cortex (Fig. 6c, areas 32, 24, and 10).

### Auditory and visual evoked potentials recorded in the primary auditory and visual areas

Robust auditory evoked potentials were recorded from the most caudal recording site on the STP array, which was estimated to be located on the primary auditory cortex in the lateral sulcus (Fig. 7a). The latency of the averaged evoked potential was short (~10 ms). There was a substantial increase in high-gamma power after stimulus onset (Fig. 7b, upper panel). These response properties were similar to the auditory evoked potentials recorded in a previous study with ECoG arrays implanted in the lateral sulcus (Fukushima et al. 2012). The other recording sites on the STP array also recorded robust auditory evoked potentials (Fig. 7c), showing increase in the response latency from caudal to rostral recording sites.

In the primary visual cortex (Fig. 7d), the first peak of the averaged evoked potential appeared at around 120 ms, comparable to the average visual response latency previously recorded with other methods (Raiguel et al. 1989; Rubehn et al. 2009). Auditory evoked potentials were recorded five months after the electrode implantation (Fig. 7b and c), and visual evoked potentials were recorded 6 months after the implantation (Fig. 7d). These results indicate the viability of the ECoG array as a tool for monitoring sensory responses from cortices belonging to different sensory modalities over a period of several months.

### Substantially reduced chewing artifacts in bipolar compared to monopolar recording

ECoG recording can be performed under restraint-free conditions without artifacts produced by motion-related noise and power-line noise. Even when noise level is relatively low, however, spontaneous noise and chewing movements often contaminate the ECoG signal (Shimoda et al. 2012). Consistent with the results of the previous study, we found a significant amount of chewing artifact in monopolar recording from the visual cortex (at the same recording location as that yielding the visual evoked potential in Fig. 7d), where no mastication-related neural activity was expected (Fig. 8, upper panels). Chewing hard foods (banana chips) produced ~8x greater peak $\Delta^2$ artifact (Fig. 8b) than chewing soft foods (raisins) (Fig. 8a). Bipolar recording successfully removed this chewing artifact for both hard and soft foods (Fig. 8, lower panels). The $\Delta^2$ in non-chewing periods had substantially smaller amplitudes in bipolar than in monopolar recording, as noted in the scale change in the lower plots of Fig. 8. This, however, does not imply an inability to extract signals through bipolar recording, since robust visual evoked potentials were detected by such recordings at the very same sites (Fig. 7d).

## Discussion

We developed a new ECoG electrode array for chronic, simultaneous recording of neural activity from numerous gyral and intrasulcal cortical areas simultaneously in rhesus monkeys. Although, conventionally, extracellular recording in monkeys is performed in only one or a few cortical areas, there have also been attempts to record simultaneously from several cortical areas. One of the pioneering studies that recorded simultaneously from multiple sensory and motor areas using 15 bipolar penetrating electrodes (Bressler et al. 1993; Bressler and Nakamura 1993). Later, ECoG was used to record simultaneously from multiple visual cortical areas with stainless-steel electrodes in anesthetized monkeys (Rols et al. 2001). More recently, a chronically implantable ECoG array with platinum electrodes

covered with silicone film was developed for recording neural activity from awake behaving monkeys (Chao et al. 2010). Finally, recent advances in MEMS processing has enabled the fabrication of high-density ECoG on thin films (Rubehn et al. 2009; Toda et al. 2011), allowing for easier insertion into intrasulcal cortex (Matsuo et al. 2011; Fukushima et al. 2012). By combining these features, we developed and successfully implanted an ECoG array that covered nearly the entire lateral surface and medial wall of the hemisphere, together with the supratemporal plane in the lateral sulcus.

The compartmental design of the array provided flexibility in the implantation procedure. In previous studies with intrasucal ECoG arrays, additional electrodes were placed on the inferior temporal gyrus (Matsuo et al. 2011) or the superior temporal gyrus (Fukushima et al. 2012). In the current study, the array covered gyral areas far more extensively than those in the two previous studies, therefore we designed the electrode array so that the cables from the sulcal electrodes would fit around the gyral electrodes and cables covering the lateral surface. As this was difficult to achieve with the one-sheet design used in previous ECoG arrays (Rubehn et al. 2009; Nagasaka et al. 2011), we designed the present one with finger strips of electrodes and four separate compartments (Fig. 2b). The design allowed us to first place the electrodes in the lateral sulcus and then to cover the lateral surface with other electrodes (see Material and methods). The spaces between the finger strips of compartments #3 and #4 provided multiple exit points for the cables from the lateral sulcus to accommodate anatomical differences among the animals. This design would also be useful to implant the intrasulcal electrodes to other sulcus (e.g. superior temporal sulcus) (Matsuo et al. 2011). The compartmental design also enabled flexibility in combining different compartments according to recording requirements, despite a limited number of recording channels. In addition, this design would allow replacing some of the electrode compartments with others having different patterns of ECoG electrodes or chronically implantable penetrating electrode arrays.

Although the connector enclosure stored more than 256 pins, it occupies only a small space (10 mm x 23 mm), leaving sufficient room on the skull to increase the number of electrodes channels and still leave space for the head post needed to stabilize the animal's head during a recording session. The large number of channels allowed for extraction of information at a finer spatial resolution from a large extent of cortex. The overall electrode density in our ECoG array is relatively sparse compared to ECoG arrays made with MEMS technologies and used previously in macaques (Rubehn et al. 2009; Matsuo et al. 2011; Fukushima et al. 2012). The ECoG array in the current study had a bipolar inter-electrode distance of 1.8 mm (Fig. 2a). The distance between bipolar pairs was ~5 mm, which is comparable to that in a silicon sheet ECoG array (Nagasaka et al. 2011). Although increasing the electrode density with the same electrode size (1 mm) did not improve decoding performance significantly (Chao et al. 2010), it enabled detection of fine functional subdivisions in auditory and visual cortex due to the smaller contact size (50 μm diameter) (Fukushima et al. 2012) or to the use of bipolar rather than monopolar electrodes with the same contact size (1 mm diameter) (Rubehn et al. 2009). Thus, combining a higher density ECoG array with smaller contact size in bipolar configuration could help to extract spatially finer information. In addition, local referencing of signals with bipolar recording avoided contamination from volume-conducted potentials from distant sites (Kajikawa and Schroeder 2011), as evidenced by

elimination of chewing artifacts by recording with bipolar rather than with monopolar electrodes (Fig. 8). The ECoG array can be improved further by multiplexing recording signals to support a higher number of recording sites (Viventi et al. 2011). Finally, for better biocompatibility, gold plating could be replaced by platinum and the support of the electrodes could be changed to other materials (e.g. silicon film).

## Conclusions

We developed and successfully implanted a compartmentlized ECoG electrode array to record electrical field potentials simultaneously from most of the lateral cortex, parts of the medial wall, and a large extent of the supratemporal plane in the lateral sulcus. This modification of the ECoG array compared to previously used versions expands the number of cortical target areas that can be recorded simultaneously. We successfully recorded auditory evoked potentials from the primary auditory cortex in the lateral sulcus, as well as visual evoked potentials from the primary visual cortex on the lateral surface of the occipital lobe. The compartmentalized ECoG array provides an opportunity to investigate global network interactions among gyral and intrasulcal cortical areas underlying, for instance, multisensory processing and concomitant behavior (Ghazanfar and Schroeder 2006). It also enables investigating global network interactions that underlie vocalization, an oromotor function that requires the participation of multiple cortical areas for both producing and processing self-generated sounds (Fukushima et al. in press).

## Acknowledgments

We thank T Shirayanagi for technical assistance in electrode design and schematics of the array, D Johnson for assistance with CT scans, R Reoli for assistance with MR scans, D Glen for assistance in co-registration of the CT and MR scans with AFNI, and D Rickrode for animal care. This research was supported by the Intramural Research Program of the National Institute of Mental Health (NIMH), NIH, DHHS, and by a Grant-in-Aid for Scientific Research on Innovative Areas (23118003; Adolescent Mind & Self-Regulation) and the Strategic Research Program for Brain Science by MEXT, Japan.

## References

Asaad WF, Eskandar EN. Achieving behavioral control with millisecond resolution in a high-level programming environment. J Neurosci Methods. 2008 Aug 30; 173(2):235–40. [PubMed: 18606188]

Beauchamp MS, Sun P, Baum SH, Tolias AS, Yoshor D. Electrocorticography links human temporoparietal junction to visual perception. Nat Neurosci Nature Publishing Group. 2012 Jun 3; 15(7):957–9.

Bendor D, Wang X. Neural response properties of primary, rostral, and rostrotemporal core fields in the auditory cortex of marmoset monkeys. J Neurophysiol. 2008 Aug 1; 100(2):888–906. [PubMed: 18525020]

Bosman CA, Schoffelen J-M, Brunet N, Oostenveld R, Bastos AM, Womelsdorf T, et al. Attentional Stimulus Selection through Selective Synchronization between Monkey Visual Areas. Neuron Elsevier Inc. 2012 Sep 6; 75(5):875–88.

Bressler SL, Coppola R, Nakamura R. Episodic multiregional cortical coherence at multiple frequencies during visual task performance. Nature. 1993 Nov 11; 366(6451):153–6. [PubMed: 8232553]

Bressler, SL.; Nakamura, R. Inter-area synchronization in macaque neocortex during a visual pattern discrimination task. In: FE; JB, editors. Computation and Neural Systems. Norwell, MA: Kluwer Academic Publishers; 1993. p. 515-22.

Bressler SL, Seth AK. Wiener–Granger Causality: A well established methodology. NeuroImage Elsevier Inc. 2011 Sep 15; 58(2):323–9.

Brovelli A, Ding M, Ledberg A, Chen Y, Nakamura R, Bressler S. Beta oscillations in a large-scale sensorimotor cortical network: Directional influences revealed by Granger causality. P Natl Acad Sci Usa. 2004; 101(26):9849–54.

Canolty, RT.; Knight, RT. The functional role of cross-frequency coupling. In: Regul, editor. Trends Cogn Sci. Vol. 14. Elsevier Ltd; 2010 Nov 1. p. 506-15.

Chang, EF.; Niziolek, CA.; Knight, RT.; Nagarajan, SS.; Houde, JF. Human cortical sensorimotor network underlying feedback control of vocal pitch. Proceedings of the National Academy of Sciences; 2013 Jan 23;

Chao ZC, Nagasaka Y, Fujii N. Long-term asynchronous decoding of arm motion using electrocorticographic signals in monkeys. Front Neuroengineering. 2010; 3:3.

Cox RW. AFNI: software for analysis and visualization of functional magnetic resonance neuroimages. Comput Biomed Res. 1996 Jun; 29(3):162–73. [PubMed: 8812068]

Edwards E, Soltani M, Kim W, Dalal SS, Nagarajan SS, Berger MS, et al. Comparison of Time-Frequency Responses and the Event-Related Potential to Auditory Speech Stimuli in Human Cortex. J Neurophysiol. 2009 Jul 1; 102(1):377–86. [PubMed: 19439673]

Einevoll GT, Kayser C, Logothetis NK, Panzeri S. Modelling and analysis of local field potentials for studying the function of cortical circuits. Nat Rev Neurosci Nature Publishing Group. 2013 Nov 1; 14(11):770–85.

Feingold J, Desrochers TM, Fujii N, Harlan R, Tierney PL, Shimazu H, et al. A system for recording neural activity chronically and simultaneously from multiple cortical and subcortical regions in nonhuman primates. J Neurophysiol. 2012 Apr; 107(7):1979–95. [PubMed: 22170970]

Formisano E, Kim D, Di Salle F, van de Moortele P, Ugurbil K, Goebel R. Mirror-symmetric tonotopic maps in human primary auditory cortex. Neuron. 2003; 40(4):859–69. [PubMed: 14622588]

Fries P. A mechanism for cognitive dynamics: neuronal communication through neuronal coherence. Trends Cogn Sci (Regul Ed). 2005 Oct; 9(10):474–80. [PubMed: 16150631]

Friston, K.; Moran, R.; Seth, AK. Curr Opin Neurobiol. Elsevier Ltd; 2012 Dec 18. Analysing connectivity with Granger causality and dynamic causal modelling; p. 1-7.

Fukushima, M.; Saunders, RC.; Fujii, N.; Averbeck, BB.; Mishkin, M. Modeling vocalization with ECoG cortical activity recorded during vocal production in the macaque monkey. Conference proceedings: Annual International Conference of the IEEE Engineering in Medicine and Biology Society IEEE Engineering in Medicine and Biology Society; (in press)

Fukushima M, Saunders RC, Leopold DA, Mishkin M, Averbeck BB. Spontaneous high-gamma band activity reflects functional organization of auditory cortex in the awake macaque. Neuron. 2012 Jun 7; 74(5):899–910. [PubMed: 22681693]

Fukushima M, Saunders RC, Leopold DA, Mishkin M, Averbeck BB. Differential coding of conspecific vocalizations in the ventral auditory cortical stream. J Neurosci. 2014 Mar 26; 34(13): 4665–76. [PubMed: 24672012]

Ghazanfar AA, Schroeder CE. Is neocortex essentially multisensory? Trends Cogn Sci (Regul Ed). 2006; 10(6):278–85. [PubMed: 16713325]

Giraud A-L, Poeppel D. Cortical oscillations and speech processing: emerging computational principles and operations. Nat Neurosci Nature Publishing Group. 2012 Mar 18; 15(4):511–7.

Hackett TA. Information flow in the auditory cortical network. Hear Res. 2011 Jan; 271(1–2):133–46. [PubMed: 20116421]

Kajikawa Y, Schroeder CE. How Local Is the Local Field Potential? Neuron Elsevier Inc. 2011 Dec 8; 72(5):847–58.

Kikuchi Y, Horwitz B, Mishkin M. Hierarchical auditory processing directed rostrally along the monkey's supratemporal plane. J Neurosci. 2010 Sep 29; 30(39):13021–30. [PubMed: 20881120]

Kravitz DJ, Saleem KS, Baker CI, Mishkin M. A new neural framework for visuospatial processing. 2011 Apr 1.:1–14.

Kravitz DJ, Saleem KS, Baker CI, Ungerleider LG, Mishkin M. The ventral visual pathway: an expanded neural framework for the processing of object quality. Trends Cogn Sci. 2013 Jan; 17(1):26–49. [PubMed: 23265839]

Matsuo T, Kawasaki K, Osada T, Sawahata H, Suzuki T, Shibata M, et al. Intrasulcal electrocorticography in macaque monkeys with minimally invasive neurosurgical protocols. Front Syst Neurosci. 2011; 5:34. [PubMed: 21647392]

Mesgarani, N.; Chang, EF. Nature. Nature Publishing Group; 2012 Apr 18. Selective cortical representation of attended speaker in multi-talker speech perception; p. 1-5.

Nagasaka, Y.; Shimoda, K.; Fujii, N. Multidimensional Recording (MDR) and Data Sharing: An Ecological Open Research and Educational Platform for Neuroscience. In: de Polavieja, GG., editor. PLoS ONE. Vol. 6. 2011 Jul 21. p. e22561

Nelson MJ, Pouget P, Nilsen EA, Patten CD, Schall JD. Review of signal distortion through metal microelectrode recording circuits and filters. J Neurosci Methods. 2008 Mar 30; 169(1):141–57. [PubMed: 18242715]

Palmini A. The concept of the epileptogenic zone: a modern look at Penfield and Jasper's views on the role of interictal spikes. Epileptic Disord. 2006 Aug 1; 8( Suppl 2):S10–5. [PubMed: 17012068]

Raiguel SE, Lagae L, Gulyàs B, Orban GA. Response latencies of visual cells in macaque areas V1, V2 and V5. Brain Res. 1989 Jul 24; 493(1):155–9. [PubMed: 2776003]

Rols G, Tallon-Baudry C, Girard P, Bertrand O, Bullier J. Cortical mapping of gamma oscillations in areas V1 and V4 of the macaque monkey. Visual Neurosci. 2001; 18(4):527–40.

Romanski LM, Tian B, Fritz J, Mishkin M, Goldman-Rakic PS, Rauschecker JP. Dual streams of auditory afferents target multiple domains in the primate prefrontal cortex. Nat Neurosci. 1999 Dec; 2(12):1131–6. [PubMed: 10570492]

Rubehn B, Bosman C, Oostenveld R, Fries P, Stieglitz T. A MEMS-based flexible multichannel ECoG-electrode array. J Neural Eng. 2009 May 12.6(3):036003. [PubMed: 19436080]

Saad ZS, Glen DR, Chen G, Beauchamp MS, Desai R, Cox RW. A new method for improving functional-to-structural MRI alignment using local Pearson correlation. NeuroImage. 2009 Feb 1; 44(3):839–48. [PubMed: 18976717]

Salazar RF, Dotson NM, Bressler SL, Gray CM. Content-specific fronto-parietal synchronization during visual working memory. Science. 2012 Nov 23; 338(6110):1097–100. [PubMed: 23118014]

Schmolesky MT, Wang Y, Hanes DP, Thompson KG, Leutgeb S, Schall JD, et al. Signal timing across the macaque visual system. J Neurophysiol. 1998 Jun; 79(6):3272–8. [PubMed: 9636126]

Schroeder CE, Lakatos P. Low-frequency neuronal oscillations as instruments of sensory selection. Trends Neurosci. 2009; 32(1):9–18. [PubMed: 19012975]

Scott BH, Malone BJ, Semple MN. Transformation of temporal processing across auditory cortex of awake macaques. J Neurophysiol. 2011 Feb 1; 105(2):712–30. [PubMed: 21106896]

Shimoda K, Nagasaka Y, Chao ZC, Fujii N. Decoding continuous three-dimensional hand trajectories from epidural electrocorticographic signals in Japanese macaques. J Neural Eng. 2012 May 25.9(3):036015. [PubMed: 22627008]

Toda H, Suzuki T, Sawahata H, Majima K, Kamitani Y, Hasegawa I. Simultaneous recording of ECoG and intracortical neuronal activity using a flexible multichannel electrode-mesh in visual cortex. NeuroImage. 2011; 54(1):203–12. [PubMed: 20696254]

Truccolo W, Donoghue JA, Hochberg LR, Eskandar EN, Madsen JR, Anderson WS, et al. Single-neuron dynamics in human focal epilepsy. Nat Neurosci. 2011 May; 14(5):635–41. [PubMed: 21441925]

Ungerleider, LG.; Mishkin, M. Two cortical visual systems. In: Ingle, MA.; Goodale, MI.; Masfield, R., editors. Analysis of Visual Behavior. Cambridge, MA: MIT Press; 1982. p. 549-86.

Viventi J, Kim D-H, Vigeland L, Frechette ES, Blanco JA, Kim Y-S, et al. teChnICal repOrtS. Nat Neurosci Nature Publishing Group. 2011 Nov 13; 14(12):1599–605.

Yanagisawa T, Hirata M, Saitoh Y, Kato A, Shibuya D, Kamitani Y, et al. Neural decoding using gyral and intrasulcal electrocorticograms. NeuroImage. 2009 May 1; 45(4):1099–106. [PubMed: 19349227]

## Highlights

- ECoG array for recording from multiple gyral and intrasulcul cortical areas simultaneously
- Compartmental design of the array allowed flexibility in implantation procedure
- The array detected robust auditory and visual evoked potentials in an awake monkey

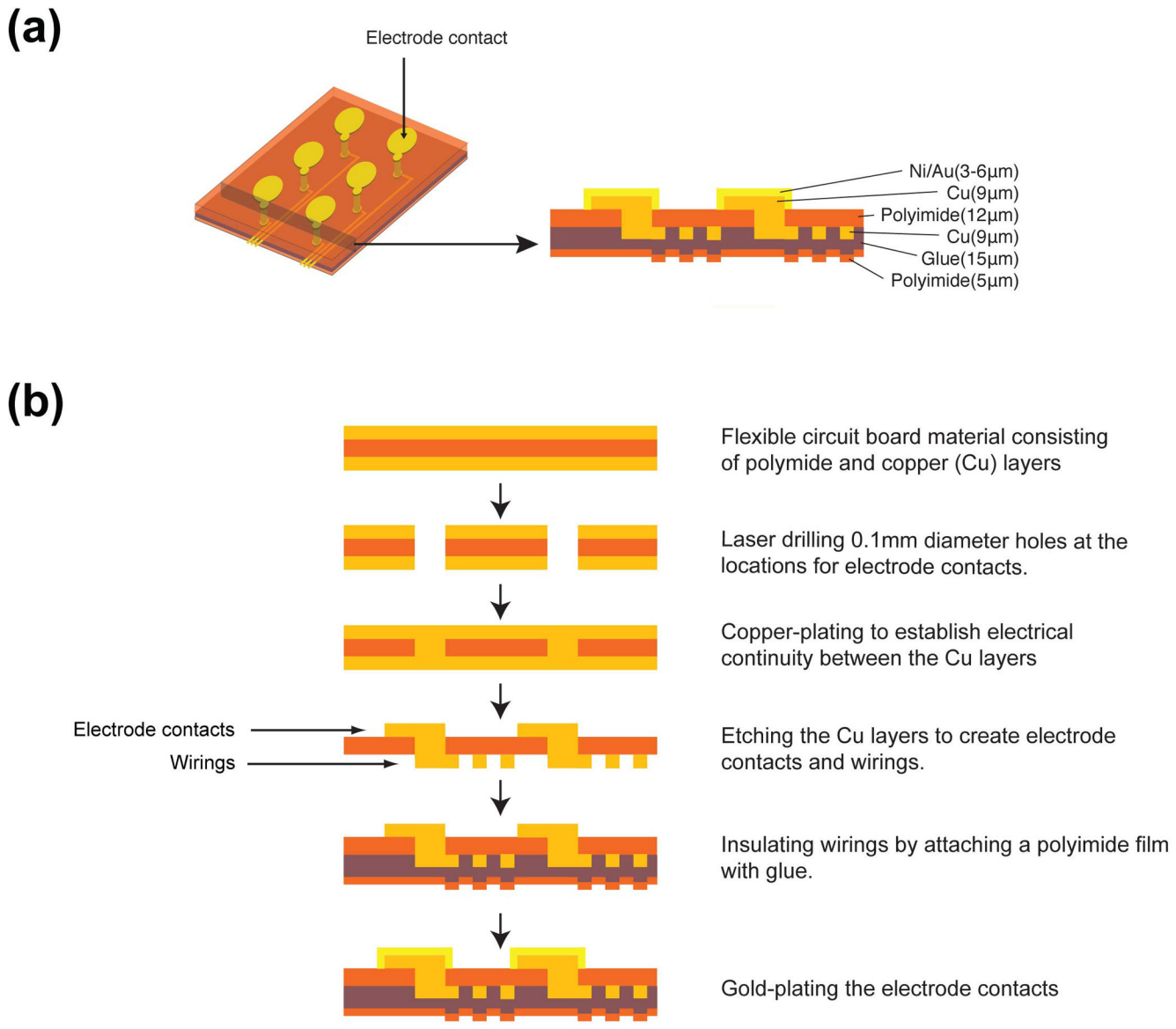


**Figure 1. Layer structure and manufacturing process of the ECoG array**

**(a)** Schematic representation of a section of the array with six electrodes. The total thickness of the electrode is 53–56 μm. **(b)** Stepwise description of the manufacturing process with microelectromechanical system (MEMS) technologies.

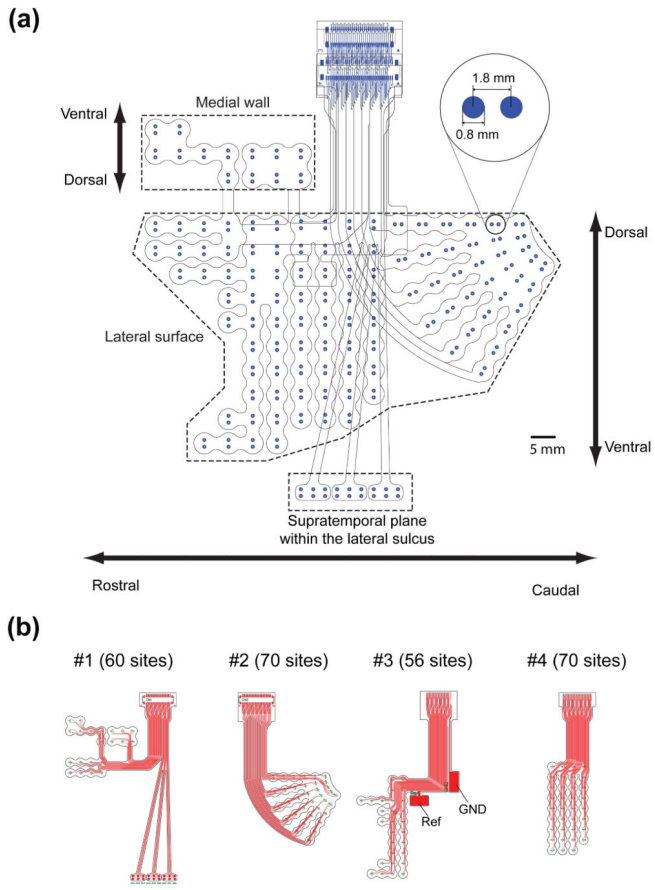


**Figure 2. Schematic representation of the ECoG array**

**(a)** Spatial layout of all 256 electrodes. The three sections outlined by the dashed lines, were designed for the medial wall (26 electrodes), the lateral surface (212 electrodes), and the supratemporal plane of the lateral sulcus (18 electrodes, STP array), respectively. A pair of electrodes designed for bipolar recording is magnified in the inset. The electrode diameter was 0.8 mm and the distance between the electrodes in the pair was 1.8 mm. The electrodes at the bottom of the lateral-surface section were designed for the ventrolateral surface, and the electrodes at the bottom of the medial-wall section were designed for the dorsolateral surface (See Fig. 6). **(b)** The four compartments (#1–4) of the array are each connected to a separate connector. Each compartment contains 56–70 electrodes.

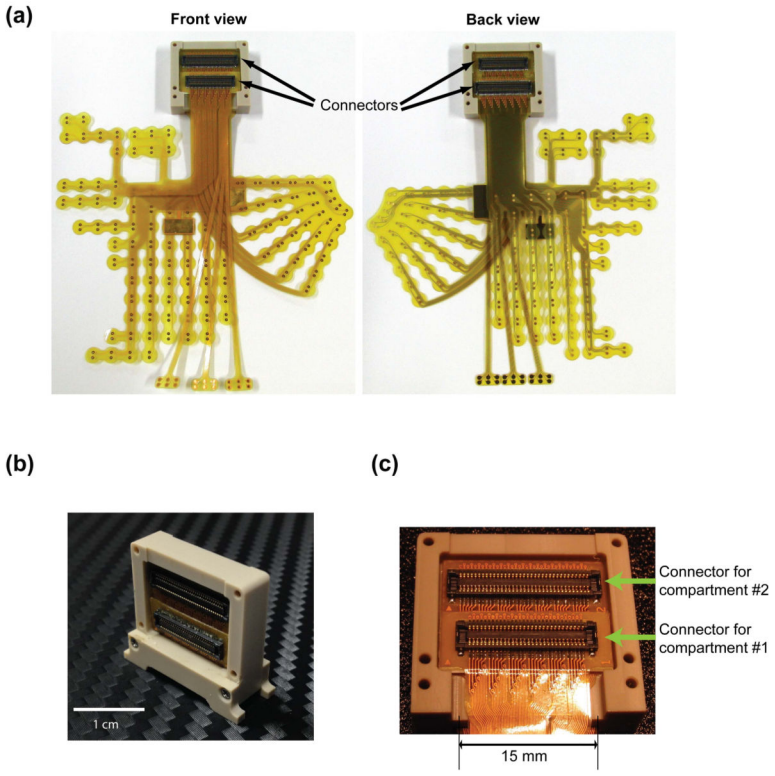


**Figure 3. The assembled ECoG electrode array and connector**

**(a)** The complete electrode assembly viewed from front (left) and back (right). Two of the four connectors (indicated by arrows) were placed on each side of the assembly. **(b)** The electrode connector enclosure with legs; two connectors can be seen on each side stacked vertically. **(c)** A magnified view of the two connectors in the front side of the enclosure. These connectors are for compartments #1 and #2. The total width of the cable is 15 mm.

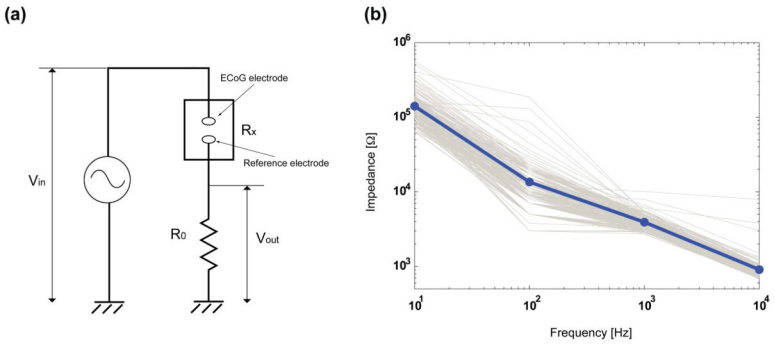


**Figure 4. Impedance measurement of the ECoG array**

**(a)** Diagram of the voltage divider circuit used for impedance measurement. The ECoG electrode and reference electrode were electrically coupled by immersion in 0.9% saline solution at room temperature. $V_{in}$: sinusoidally modulated input voltage with 0.1 mV RMS. $R_0$: resistor with known resistance values (1kΩ for 10 and 100 Hz, 1 MΩ for 1 and 10 kHz). $V_{out}$: the output voltage measured by coupling with a high input impedance amplifier. $R_X$: impedance of the electrode. **(b)** Impedance spectrum for each of the 256 electrodes (gray lines) and the mean spectrum of all electrodes (blue line).

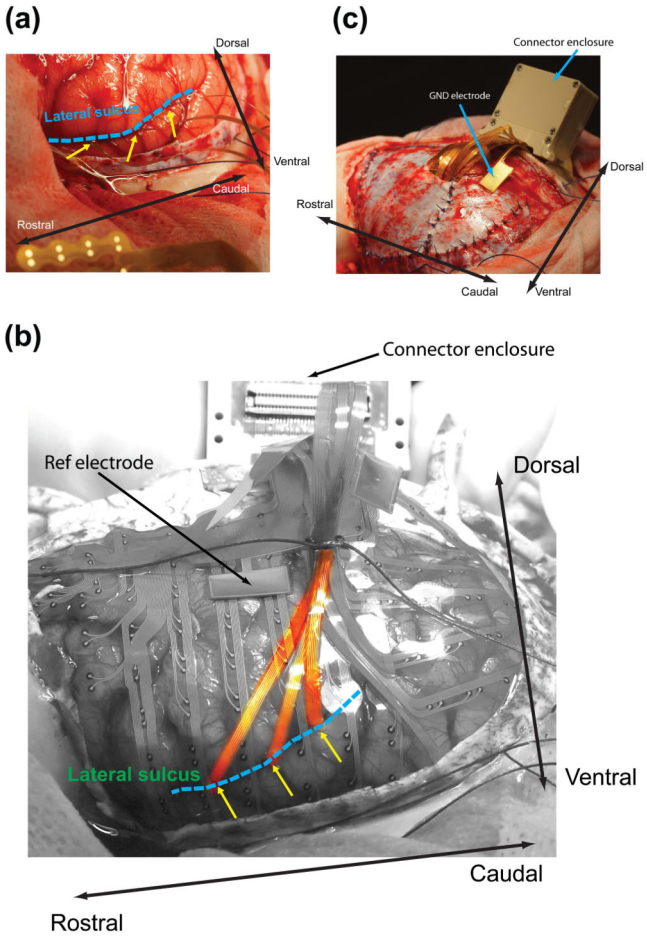


**Figure 5. Implantation of the ECoG array**

**(a)** Electrodes placed in the lateral sulcus. Eighteen electrodes were inserted onto the supratemporal plane of the lateral sulcus (blue dotted line). The cables from the electrodes exited from the sulcus at three locations (yellow arrows). **(b)** Electrodes on the lateral surface. The three cables (highlighted in red) from the lateral sulcus (blue dotted line) passed through the gaps between the electrode arrays on the lateral surface (yellow arrows). The reference (Ref) electrode was placed in the subdural space, facing the dura. **(c)** Dura sutured after placing all the electrodes. The ground (GND) electrode was placed in the epidural space, facing the bone flap.

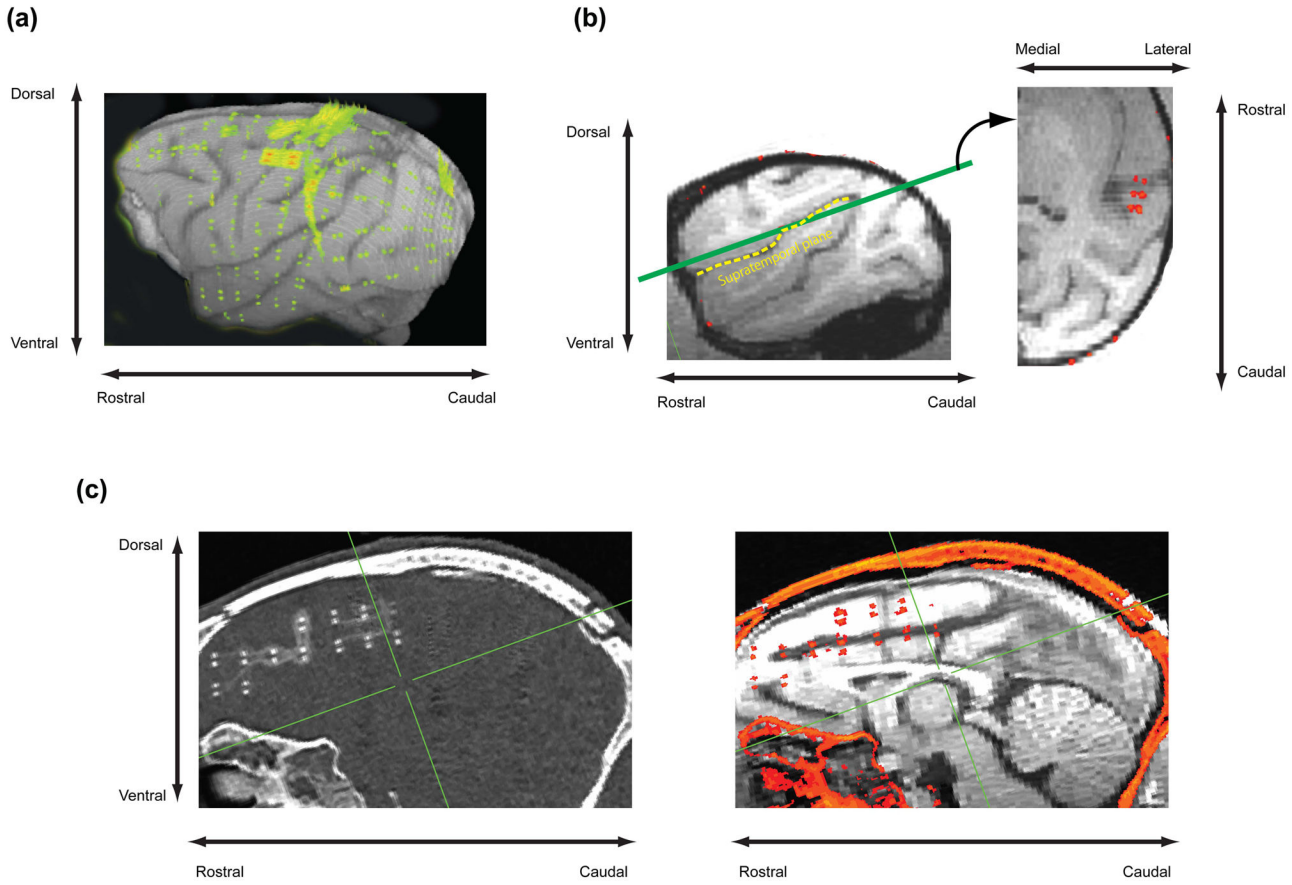


**Figure 6. Confirmation of implanted electrode locations by CT and MR scans**

**(a)** Electrodes located on the lateral surface viewed on a 3D rendered MR image of the brain. The electrodes and cables detected by a CT scan are depicted in yellow. **(b)** Electrodes implanted in the lateral sulcus. **Left,** A parasagittal brain section showing location of the electrodes (yellow) on the supratemporal plane within the lateral sulcus. **Right,** horizontal section corresponding to the green line on the parasagittal section to the left. Three pairs of electrodes can be detected in this section, in red along with cross section of skull. **(c)** Electrodes on the medial wall. **Left,** a CT scan of the section showing the electrodes. **Right,** the same CT scan co-registered with a parasagittal MRI section (electrodes and cross section of skull, in red).

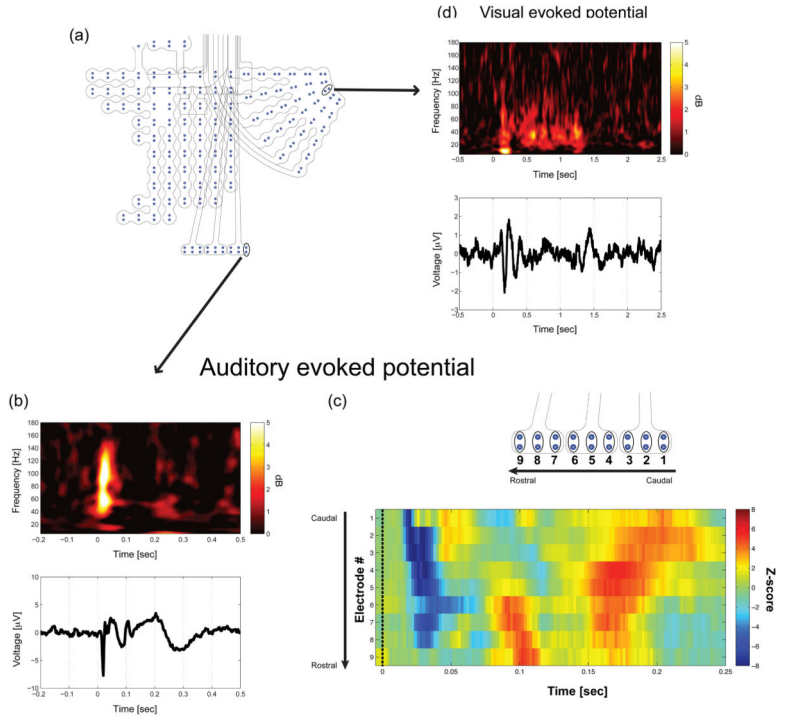


**Figure 7. Event related potentials recorded from auditory and visual cortex**

Evoked responses were calculated from differential LFPs recorded with bipolar electrodes. **(a)** Location of the two bipolar electrodes (circled) that yielded the examples of auditory and visual evoked potentials in (b) and (c), respectively. The ECoG array is the same as that shown in Fig. 2a. **(b)** Example of an evoked potential to an auditory stimulus (a 74-msec harmonic complex tone with a fundamental frequency of 500 Hz). **Upper panel,** the trial-averaged spectrogram of the evoked potential recorded from a bipolar electrode located in the primary auditory cortex on the STP of the lateral sulcus. The activity is normalized to the baseline activity recorded before the onset of the stimulus. **Lower panel,** the trial-averaged waveform of the evoked response **(c)** Examples of evoked potentials from 9 bipolar recording sites in the ECoG array implanted on the STP. The auditory stimulus used is the one in as (b). **Upper panel,** the 9 recording sites on STP. Recording site #1 is located in the most caudal part of this intrasulcal array. These 9 sites span more than 2cm in the caudorostral direction of the STP. **Lower panel,** the trial-averaged waveforms of the auditory evoked potentials recorded from the 9 sites. The magnitude of the evoked potential is normalized by calculating z-scores for each site. **(d)** Example of an evoked response to a visual stimulus (white square flashed for 1 second). **Upper panel,** the trial-averaged spectrogram of the evoked potential recorded from a bipolar electrode located in the primary visual cortex. This activity is normalized to the baseline activity recorded before the onset of the stimulus. **Lower panel,** the trial-averaged waveform of the evoked response.

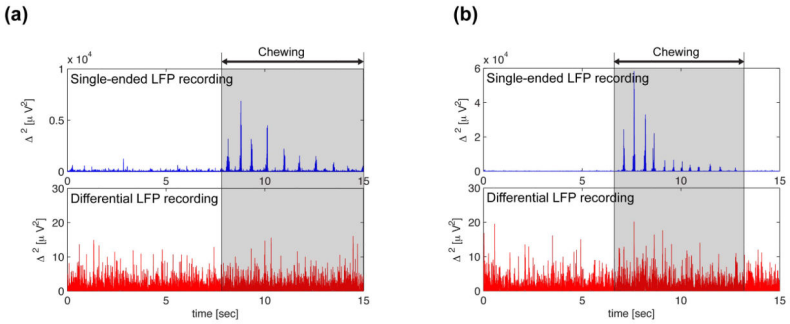


**Figure 8. Examination of chewing artifacts recorded with monopolar and bipolar electrodes**

The squared difference between the raw and smoothed field potential ($\Delta^2$, see Materials and methods), recorded from the visual cortex (at the same location as that yielding the visual evoked potential in Fig. 7d.). Gray shaded area indicates the period of mastication. **Upper panels,** $\Delta^2$ calculated from monopolar recording. **Lower panels,** differential $\Delta^2$ calculated from bipolar recordings. The monkey had been chewing soft food (raisins) in **(a)** and hard food (banana chips) in **(b).**